Transition Metal Oxide Work Functions: The Influence of Cation Oxidation State and Oxygen Vacancies

Mark T. Greiner, Lily Chai, Michael G. Helander, Wing-Man Tang, and Zheng-Hong Lu*

Transition metal oxides are capable of a wide range of work functions. This quality allows them to be used in many applications that involve charge transfer with adsorbed molecules, for example as heterogeneous catalysts, as charge-injection layers in organic electronics, and as electrodes in fuel cells. Chemical and structural factors can alter transition-metal oxide work functions, often making their work functions difficult to control. Little is known about the effects of the cation oxidation state and point defects on the oxide work function. It is necessary to understand how such chemical and structural factors affect work functions in order to controllably tune transition metal oxides for desired applications. Here, a correlation between the oxide work function and cation oxidation state is demonstrated. This correlation is attributed to the change in cation electronegativity with oxidation state. A model is presented that relates the work function to the oxygen deficiency for d^0 oxides in the limit of dilute oxygen vacancies. It is proposed that the rapid initial decrease in work function, observed for d^0 oxides, is caused by an increase in the density of donor-like defect states. It is also shown that oxides tend to have decreased work functions near a metal/metal-oxide interface as a consequence of the relationship between defects and work function. These insights provide guidelines for tuning transition metal oxide work functions.

1. Introduction

Transition metal oxides are useful in a wide range of applications. For example, they are used as: heterogeneous catalysts in industrial chemical processing,[1] photo-catalysts in artificial photosynthesis,[2] charge-injection layers in organic electronics devices[3] and as electrodes in fuel cells. In each of these applications, transition metal oxides are involved in charge exchange with adsorbed molecules.

Charge exchange, between a solid and an adsorbed molecule—´, depends critically on the solid's work function (φ).[4,5] When tailoring solid materials for applications that involve interfacial charge-exchange, understanding how to tune a solid material's work function is paramount. Transition metal oxide work functions can range from the extreme low ($\varphi \approx 3$ eV for ZrO_2) to the extreme high ($\varphi \approx 7$ eV for V_2O_5).[6]

Dr. M. T. Greiner, L. Chai, Dr. M. G. Helander,
Dr. W.-M. Tang, Prof. Z.-H. Lu
Department of Materials Science and Engineering
University of Toronto
184 College Street, Toronto, Ontario, M5S 3E4, Canada
E-mail: mark.greiner@mail.utoronto.ca

DOI: 10.1002/adfm.201200615

Many factors contribute to transition-metal oxide chemical and electronic properties. For instance, many transition metals have more than one stable oxidation state, and thus have multiple stable oxides. The oxides can range from insulating to semiconducting to metallic.[7] Oxides also exhibit doping asymmetry, as a result of their propensity for different types of defects.[8] Defects often give rise to a change in cation valence state. These cations can act as n- or p-type dopants. Oxygen vacancies usually act as n-type dopants. At very high oxygen vacancy concentrations, oxides can be reduced to form new stable phases that contain only low-oxidation-state cations. It is well known that defects and cation oxidation state strongly influence a transition-metal oxide's electronic properties;[9] however, it is not established how these factors affect an oxide's work function.

Work function is an important parameter for charge-exchange because it represents the energetic requirements for adding or removing an electron to or from a solid. Work function is defined as the energy required for moving an electron from a material's Fermi level to the local vacuum level. A material's work function has two contributions: 1) electron chemical potential and 2) surface dipole,[10] as illustrated in **Figure 1**. The electron chemical potential (μ_e) represents the Fermi energy (E_F) relative to the absolute vacuum level ($E_{V\infty}$). The surface dipole (δ) represents an additional energetic barrier to removing an electron from the solid's surface. The dipole barrier can be caused by the electrostatic field formed by electron density spilling from a solid's surface, but it can also be altered by adsorption of molecules to a surface.

The work function is a property that is difficult to control due to its extreme sensitivity to a number of factors that are often beyond a scientist's control or awareness. Consequently, there is a wide spread in the reported work functions for most materials.[11,12] Surface dipole can be affected by crystallographic orientation,[13] surface termination and reconstruction, surface roughness[13,14] and the presence of adsorbates.[5] There are also many factors that can alter a solid's electron chemical potential, such as impurities, crystal structure, defects, and chemical state.

Transition-metal oxide work functions are especially difficult to reproduce due to the additional influence of multiple cation oxidation states and stoichiometry. As pointed out by Henrich

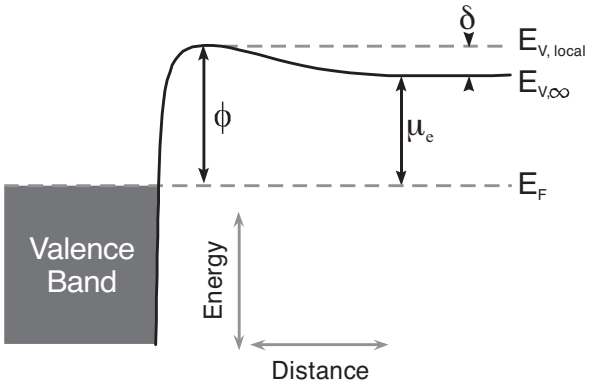

Figure 1. Illustration of energy levels near the surface of a solid, indicating work function (φ), Fermi level (E_F), surface dipole (δ), electron chemical potential (μ_e), local vacuum level ($E_{V,\,local}$), and absolute vacuum level ($E_{V,\infty}$).

and Cox in their seminal book on metal oxide surfaces,[12] there is wild inconsistency in the work function values reported for many transition metal oxides. This is primarily due to the many different sample preparation procedures that are used.

While the inconsistency of reported work-function values may lead one to the doubt the significance of absolute work functions, it is important to realize that work function is more a measure of a material's condition than a measure of a material constant. However, reproducible work function values can be obtained for some materials. For example, polycrystalline sputter-cleaned Au reproducibly has a work function of 5.35 ± 0.05 eV. Polycrystalline Cu has a work function of 4.66 ± 0.05 eV. Polycrystalline MoO_3, prepared by vacuum sublimation of MoO_3, and without exposure to adsorbates, has a work function between 6.8 and 6.9 eV.

Absolute work function values do have significance, but it is necessary to understand the factors that affect work function and how they affect it. There have been many studies on how adsorbates affect surface dipole. Atmospheric gases adsorbed to high-work-function oxides, such as MoO_3 and NiO, tend to cause a drop in work function.[15,16] However, far fewer studies have appeared in the literature regarding to how work function is affected by changing a solid's electron chemical potential. In the case of oxides, one would expect that their electron chemical potentials should change with cation oxidation state and electronic structure.

In the current report, we present work-function values for several in situ prepared transition metal oxides. We have found that there is a general correlation between cation oxidation state and an oxide's work function. Metal oxides in their more-oxidized forms tend to have higher work functions than their reduced forms. Furthermore, metal oxides tend to have higher work functions than their elemental metals.

It is not obvious why a correlation between cation oxidation state and work function should exist. Clearly high and low oxidation-state forms of an oxide differ from one another in more ways than just the cation oxidation state. Oxides also differ from one another on terms of crystal structures, bond lengths, types of bonding and degree of orbital overlap. All of these factors contribute to an oxide's valence electronic structure, and thus should affect its Fermi level. The correlation between cation oxidation state and work function implies that, aside from the many factors that give rise to the fine details of an oxide's electronic structure, oxidation state plays a relatively straight-forward role in determining an oxide's electron chemical potential.

Using the archetypal d^0 transition metal oxide MoO_3, we demonstrate how cation-oxidation-state point defects affect an oxide's work function in the limit of dilute defects. We construct a model to explain the observed trend between MoO_3's work function and O-vacancy concentration in the dilute limit. The model stipulates that the work function drop that accompanies oxide reduction are: 1) the lower electronegativity of low-oxidation-state cations alters the oxide's electron chemical potential and 2) occupied defect states within the bandgap that act as donor levels cause a shift in the Fermi level position.

The first contribution (the effect of cation electronegativity) is general to all metal oxides. The second contribution (the effect of occupied defect states in the bandgap) is not general, and only applies to oxides where gap states are formed upon O-vacancy formation. However, the formation of O-vacancy donor states is a property that is common to all d^0 oxides.

The d^0 oxides include many technologically important oxides, such as TiO_2, HfO_2, V_2O_5, ZrO_2, Ta_2O_5, WO_3 and CrO_3. The d^0 oxides tend to be wide-band-gap materials, with valence-band maxima composed primarily of O 2p states and conduction-band minima composed mainly of metal d-states.[17] These oxides contain fully oxidized transition metal cations, in which the cation's d-band is considered completely empty.

Several d^0 oxides (such as MoO_3,[18] WO_3,[19] TiO_2, ZrO_2 and V_2O_5[6]) have recently attracted considerable attention from the organic electronics community, as these oxides can be used as charge-injection buffer layers. Research in this field has provided valuable insight into the electronic structure of d^0 oxides and the role of defects in defining an oxide's electronic characteristics.[19–21]

The d^0 oxides have a tendency to form O-vacancy defects that result in filling of the d-band and give rise to occupied gap states.[22] Measurements from ultraviolet photoemission spectroscopy (UPS) and inverse photoemission spectroscopy (IPES) show that these occupied states push the Fermi level very close to the conduction band.[6,18,19,21] Consequently, these oxides tend to be n-type semiconductors. Furthermore, their low-lying conduction bands make them capable of accepting electrons from the HOMO levels of many organic semiconductors.[18,23,24] Their electronic properties can also be tuned by changing cation oxidation states. For example, by reducing the metal cations, MoO_3 and WO_3 can be made semi-metallic due to filling of the d-band.[25] This improved conductivity can be beneficial in organic devices; however, oxide reduction also changes work function, which may affect energy-level alignment. Thus it is valuable to know how work function and oxidation state are correlated.

The results in the present work show that small changes in stoichiometry give rise to significant changes in work function. After presenting a model for describing dilute defects we examine how MoO_3 behaves with high defect densities, approaching the limit of complete reduction to MoO_2. This situation is more complex because the oxide's lattice and electronic

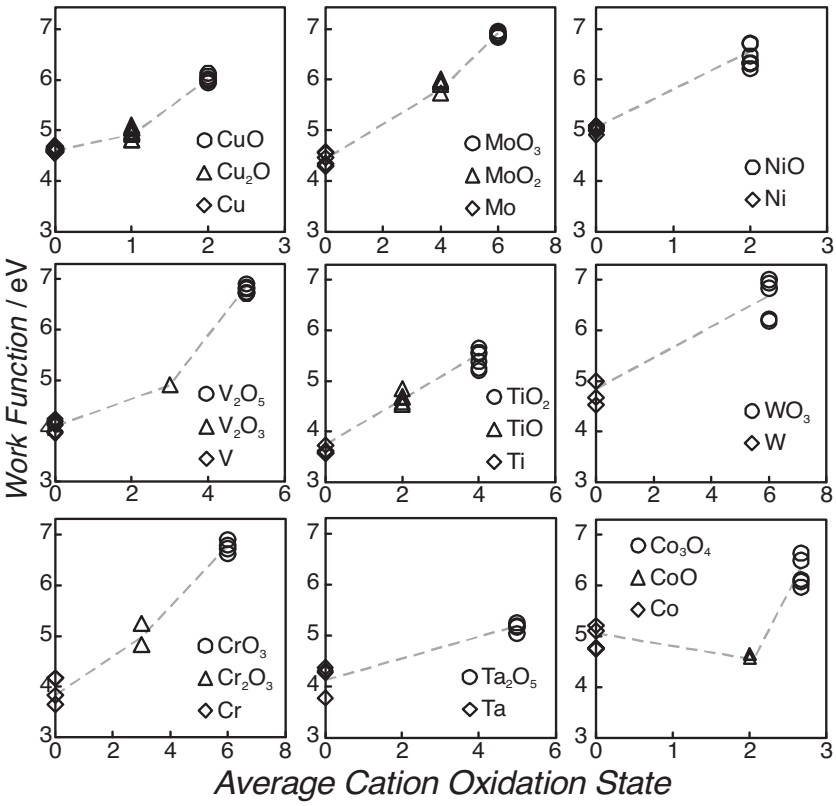

Figure 2. Plots of work function versus nominal average oxidation state of metal atoms in several transition metals and transition metal oxides. The oxides were grown as thin films via in situ oxidation. XPS and UPS spectra of each metal and metal oxide are available in Supporting Information.

structure completely change upon reduction. However, the same underlying trend is observed, where low-electronegativity cations results in a work function decrease.

We finish by demonstrating how these findings affect an oxide's work function near-by a metal interface. Oxygen vacancy defects that commonly form at metal/metal-oxide interfaces give rise to reduced metal cations near the interface, and result in a work function that is lower than that of a bulk stoichiometric oxide. These findings have implications for oxides used as injection barriers in organic electronic devices and as catalyst nano-particles in contact with metals.

2. Results and Discussion

2.1. Work Functions of Transition Metal Oxides

Plots of work function versus cation oxidation state for several transition metals and transition metal oxides are shown in **Figure 2**. These plots demonstrate that a general trend exists between transition metal cation oxidation state and work function.

The values used for Figure 2 are from photoemission measurements of thin polycrystalline oxide films, grown by in situ metal oxidation (low-oxidation state forms made by annealing oxides in vacuum). Photoemission spectra of the metals and oxides are available in Supporting Information. It is apparent from Figure 2 that there is a considerable scatter in oxide work function values. The scatter is caused by several factors. For oxide thin films, work function depends on oxide thickness, as a result of defects near the metal/metal-oxide interface. After a certain thickness, work function plateaus at a maximum value. Thus, oxide films must be sufficiently thick to obtain reproducible values.

Scatter also results from the measure of oxidation state. The oxidation state values that were used to plot Figure 2 are nominal average oxidation states. The nominal oxidation states were based on the core-level binding energies from the principle XPS peaks of the metal cations in each oxide (see Supporting Information). Thus, in determining oxidation state, we did not account for slight deviations from stoichiometry. Small concentrations of lower-oxidation-state cations may be present below the detection limit of XPS, and give rise to scatter in the work function values.

Regardless of the scatter in Figure 2, a general trend is still apparent: lower cation oxidation states generally have the effect of decreasing an oxide's work function. This trend is intriguing when one considers how oxidation state is intimately related to several other factors that affect electronic structure, such as oxide crystal structure and stoichiometry. One cannot independently change cation oxidation state without changing several other properties. Therefore it is somewhat surprising that lowering oxidation states leads to this general trend.

The fact that this trend is observed for materials with such diverse properties implies that some common effect underlies this behavior. We propose that, even though crystal structure and electron band filling do affect the Fermi level position, cation oxidation state has a dominating influence on the electron chemical potential of an oxide. The origin of this effect is caused by cation electronegativity.

2.2. Electronegativity and Fermi Level

Electronegativity is a concept that was originally proposed by Pauling in 1932. It has since proven to be very useful for explaining and predicting many chemical properties. For example, it can explain charge distribution in chemical bonds,[26] Lewis acidity,[27] dielectric properties of atoms,[28] heats of formation,[28] polarizabilities of semiconductors[29] and even mechanical properties of materials such as hardness and bulk modulus.[30]

Here we will discuss why an oxide's Fermi level depends on cation electronegativity. It has been known for many years that a linear relationship exists between the work functions

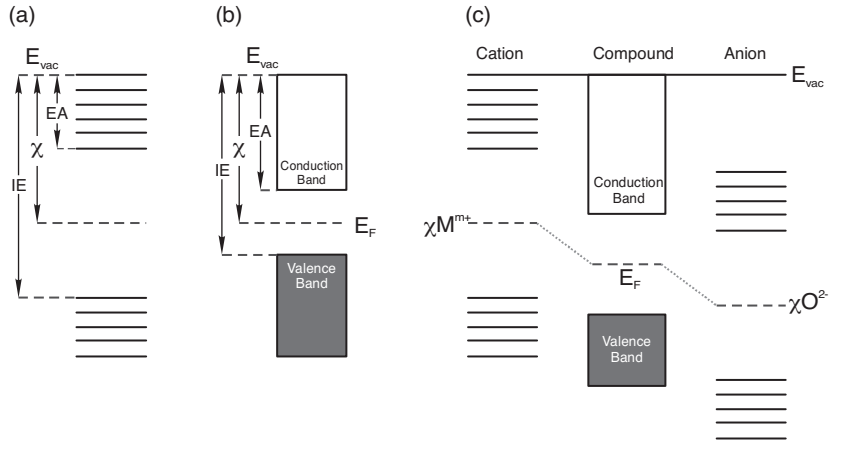

Figure 3. Illustrations of relationships between electronegativity (χ), ionization energy (IE), electron affinity (EA) and Fermi level (E_F). Schematic energy-level diagrams of a) an isolated atom, b) a condensed solid semiconductor, and c) a binary oxide (Adapted with permission from ref. [39]. Copyright 2004, Elsevier.). The electronegativity of an isolated metal cation is labeled χM^{m+} and an isolated oxygen anion labeled χO^{2-}.

of metals and their electronegativities (known as the Gordy-Thomas relation).[31] It was later realized that the work functions of semiconductors and binary compounds are also related to electronegativity values.[32,33] It is understandable why work function and electronegativity should be related. Work function represents the minimum energy needed to remove an electron of a solid, while electronegativity represents the attraction of a valence electron to an ion core.[34,35]

Mulliken's concept of electronegativity is probably the most convenient way of viewing electronegativity. Mulliken noted that electronegativity should be proportional to the average of an atom's first ionization energy and its electron affinity.[36]

$$\chi = 1/2\,(IE + EA) \tag{1}$$

Where χ is the Mulliken electronegativity, IE is ionization energy and EA is electron affinity. Mulliken's concept of electronegativity is illustrated in **Figure 3**a. In 1978, Parr et al used density functional theorem to confirmed Mulliken's concept of electronegativity, and showed that electronegativity is equivalent to the negative of electron chemical potential (i.e., the derivative of energy with respect to number of electrons).[37]

The electronegativity concept can also apply to solids. In a solid, atomic energy levels form bands. The top of the valence band is the ionization energy and the bottom of the conduction band is the electron affinity. From Mulliken's definition, electronegativity is equivalent to the mid-gap position, as shown in Figure 3b. In an un-doped semiconductor, the mid-gap is equivalent to the Fermi level when hole and electron effective masses are equal. When hole and electron effective masses are *not* equal, the deviation from mid-gap is small, even if hole and electron effective masses differ by several orders of magnitude.[38] Thus, Mulliken electronegativity is a good approximation of the Fermi level for undoped semiconductors.

The electronegativity concept is not restricted to pure elements; it also applies to compounds. In a compound, electronegativities of the constituent elements equilibrate.[26] This gives rise to group electronegativity. In 1974, Nethercott related the Fermi level of binary compounds to the electronegativities of the constituent elements by calculating group electronegativities using the postulate of geometric mean (i.e., $\chi_{AB} = (\chi_A\chi_B)^{1/2}$).[32] Accordingly, the Fermi level for the binary compound A_mB_n, where A and B represent elements and m and n represent stoichiometric coefficients, can be written as follows:

$$E_F = \left(\chi_A^m \chi_B^n\right)^{1/(m+n)} \tag{2}$$

This concept is depicted in Figure 3c. Recently, Campet et al. applied the group electronegativity concept to metal oxides, but noted that the electronegativies of metal cations and oxygen anions depend on the oxidation states of the respective ions.[39,40] In general, an atom's electronegativity is not constant. It depends on the atom's valence state.[41] Electronegativity is proportional to effective nuclear charge.[34] As oxidation state increases, so too does effective nuclear charge. Consequently, electronegativity tends to increase with oxidation state, although coordination environment also affects electronegativity.[41] Thus, in an oxide one would expect that group electronegativity, and therefore work function, should decrease with cation oxidation state.

2.3. Electronegativies and Work Functions of Transition-Metal Oxides

We have calculated the group electronegativity values of various transition-metal oxides and compared with experimental values of Fermi level. The comparison is plotted in **Figure 4**. Group electronegativity yields the mid-gap position. However, work function does not always represent the mid-gap position because in many cases oxides are p- or n-type due to intrinsic

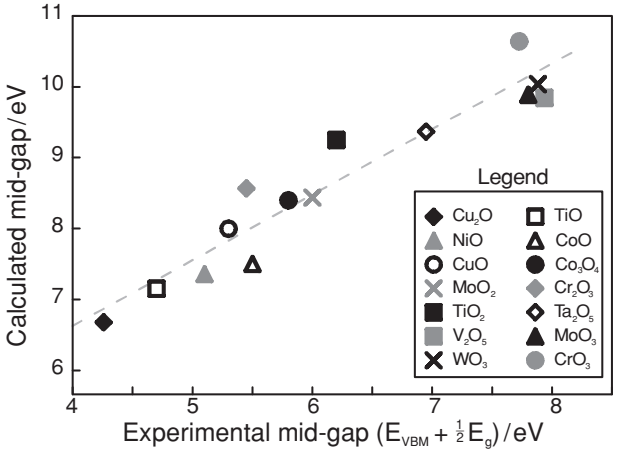

Figure 4. The calculated mid-gap positions (using ionic electronegativities) versus the experimental mid-gap positions (determined from UPS measurements and literature bandgaps) for several transition-metal oxides. The dashed line shows the linear regression.

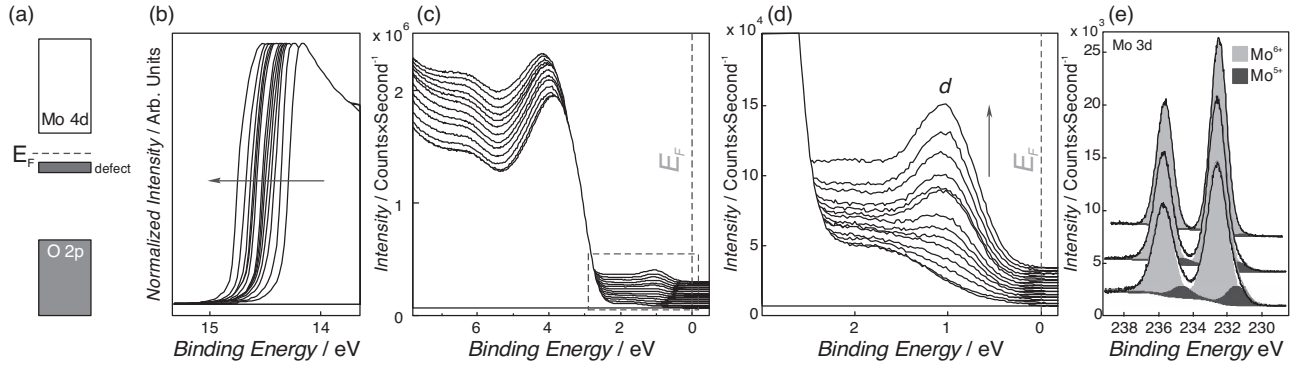

Figure 5. a) Energy-level schematic of O-deficient MoO_3, with the Fermi level (E_F), O 2p band, Mo 4d band, and defect band indicated. b–d) UV photoemission spectra of MoO_3 as oxygen vacancies are introduced: b) secondary-electron cut-off, c) valence band, and d) expanded view of the shallow valence features. The gap state resulting from the oxygen vacancy defects is labeled *d*. e) Mo 3d XPS spectra of MoO_3 as the oxygen vacancy concentration is increased (from top to bottom). The peak components from Mo^{6+} and Mo^{5+} are indicated.

defects. In order to determine the mid-gap position of these oxides, we used the valence band maximum position from UPS measurements and added half of the electronic bandgap, using literature reports of bandgap. The plot yields a reasonably linear correlation. The linear regression shown in Figure 4 has an R^2 of 0.91 and follows the relation $y = 0.925x + 2.83$.

The cation electronegativity values were taken from Matar et al.,[40] which are related to the ionic electronegativity concepts proposed by Zhang[42] and Xue.[34] The oxygen anion electronegativity depends on the electronegativity of the coordinated cations.[43] The oxygen anion electronegativities that were used to calculate group electronegativity in Figure 4 are based on Campet's method.[39] Electronegativity values were converted to electronvolt units using equations from Matar et al.[40] All electronegativity values are tabulate in the supplementary information.

We used nominal stoichiometry values for calculating the oxides' group electronegativities. Stoichiometry was determined from the core-level photoemission spectroscopy, where cation oxidation state was determined from the chemical shift of high-resolution spectra of metal cation emission peaks and these values were corroborated with peak area ratios from the O 1s spectra. Compositions were also confirmed by comparison of valence band spectra with literature reference spectra[19,21,44–49] (see Supporting Information).

The experimental mid-gap positions represent the mid-gap relative to the local vacuum level of the oxide. The experimental mid-gaps were determined using the ionization energy of the oxides' valence band maxima by adding the binding energy of the valence band edge (E_{VBM}) to the measured work function, then adding half of the electronic bandgap. Electronic bandgaps were taken from literature values of UPS and IPES measurements (TiO_2,[44] V_2O_5,[45] NiO, Cu_2O, CuO Cr_2O_5,[46] CrO_3,[47] CoO, Co_3O_4,[48] MoO_3,[21] Ta_2O_5[49] and WO_3).[19] Note that the accuracy of these bandgap measurements may vary, as they involve IPES, which only has a resolution of ≈0.5 eV and also can cause damage to the oxides during the prolonged electron exposure required for the measurements. The valence-band maxima positions are generally rather accurate (±0.1 eV).

2.4. Dilute Defects in d^0 Oxides

By examining how an oxide's work function changes when defects are introduced in dilute concentrations we can examine how low-oxidation-state cations affect an oxide's work function while causing minimal changes to the oxide's crystal structure. We can then model the observed trend using the concept of electronegativity and Nethercott's postulate of geometric mean.

We demonstrate the effect of dilute O-vacancies using the prototypical d^0 oxide, MoO_3. MoO_3 has valence and core-level photoemission spectra that are rather straight-forward to interpret. The Mo 3d XPS peaks for MoO_3 are symmetric and Gaussian-Lorenztian shaped. Lower oxidation-state forms of Mo have significant chemical shifts and tend to be slightly asymmetric.[21,50] The UPS spectrum of MoO_3 (**Figure 5**) consists of a distinct O 2p band, centered at ≈3.5 eV (binding energy). The presence of Mo^{5+} cations causes filling of the Mo 4d band, which gives rise to a distinct peak centered at ≈1eV (binding energy).

Defects were introduced using noble gas ion sputtering (see experimental section). Figure 5b–d shows how the secondary electron cut-off (used for determining work function) and the UPS valence-band spectra and of MoO_3 change as the O-vacancy concentration increases. The MoO_3 work function starts off at ≈6.9 eV for nearly stoichiometric MoO_3 and it decreases as O-vacancy concentration increases. Meanwhile, the O 2p valence band shifts to higher binding energy and a new occupied state appears within MoO_3's bandgap, labeled *d* in Figure 5. This gap state arises because, when an O^{2-} ion is removed, Mo^{6+} must be reduced to Mo^{5+} in order for charge neutrality to be maintained. As a result, MoO_3's previously empty 4d band becomes partially occupied with electrons,[51] giving rise to the defect feature seen in the valence spectra. The gap state gradually increases in size as the vacancy concentration increases.

Mo^{5+} species are also evident in the core level spectra, as shown in the Mo 3d XPS spectra in Figure 5e. The main Mo 3d peak (at 232.50 eV) is from Mo^{6+} species. As the O-vacancy concentration increases, a shoulder from Mo^{5+} appears at

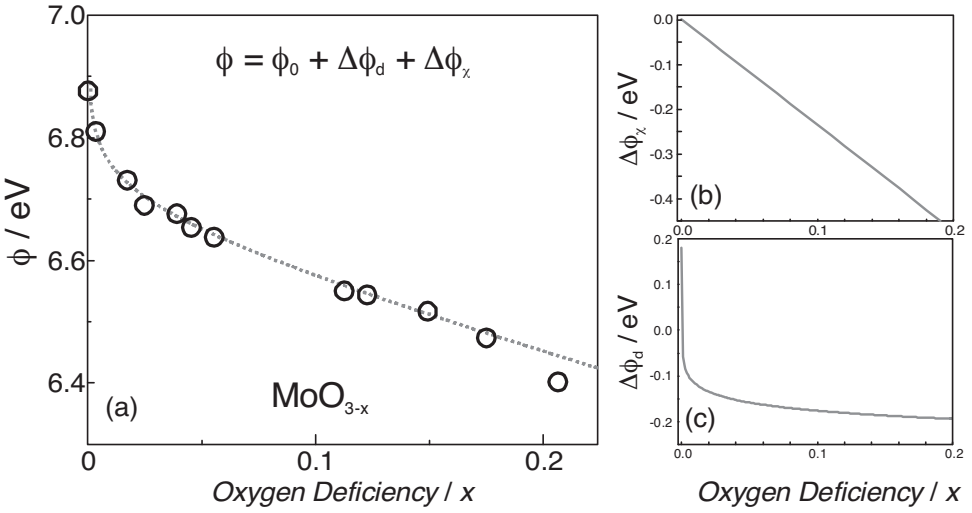

Figure 6. a) Plot of work function versus oxygen deficiency, *x*. The red circles are experimental measurements and the dashed blue curve is the predicted trend from Equation (13). The terms in the equation are: the measured work function of an O-deficient oxide, φ; the work function of a reference stoichiometric oxide, φ_0; the change in work function caused by low electronegativity cations, $\Delta\varphi_\chi$; and the change in work function caused by donor states, $\Delta\varphi_d$. b) Plot of the electronegativity contribution and c) the donor state contribution to the work function versus O-deficiency trend.

≈231.5 eV and the Mo^{6+} peak shifts towards higher binding energy (0.15 eV). We have used the Mo 3d and O 1s peak areas to determine the O-vacancy concentrations. Note that even near-stoichiometric MoO_3 contains some O-vacancies, simply due to the thermodynamic equilibrium concentration of vacancies at ambient temperatures; however, the O-vacancy concentration of near-stoichiometric MoO_3 is too small to be accurately determined by XPS.

Figure 6a shows a plot of work function versus O-deficiency as determined from the UPS spectra in Figure 5. The trend shows an initial rapid decrease in work function, followed by a more gradual and almost linear decrease. In next section we derive a model to explain this behavior. The dashed line shown in Figure 6a is based on the model (see Equation (13)).

The model stipulates that the work function decrease that accompanies O-deficiency is a result the formation of lower electronegativity cations, and an increase in the density of occupied states close to the Fermi level. It could be argued that the observed work function changes are a result of surface dipole changes. However, changes to the surface dipole would result in work function changes only; surface dipole would not affect the oxide's core or valence binding energies (discussed further in the Supporting Information). As shown in Figure 5c, the work function change is accompanied by a shift in the O 2p binding energy.

Similar experiments were performed on two other d^0 oxides (TiO_2 and WO_3) and discussed in the Supporting Information. The behavior is similar in both cases, where cation reduction is accompanied by an initial rapid work function decrease, followed by a sustained decrease. In the case of TiO_2, we used a thin TiO_2 film such that both the oxide peak (Ti^{4+}) and underlying metal peak (Ti^0) could be observed simultaneously. In this case we find that the Ti^{4+} peaks shift with work function, while the Ti^0 peak remains constant. This observation implies a shift in the Fermi level of the oxide rather than a change in the surface dipole.

2.5. Work Function, Cation Electronegativity and Donor States

From the relationship between φ and O-deficiency (x in MoO_{3-x}) shown in Figure 6a, we propose that that there are two main factors contributing to the change in MoO_3's work function: 1) increased concentration of cations with low electronegativity and 2) increased concentration of donor states. This yields the following expression for work function:

$$\phi = \phi_0 + \Delta\phi_\chi + \Delta\phi_d \tag{3}$$

where ϕ is the measured work function, ϕ_0 is the work function of the stoichiometric oxide, $\Delta\phi\chi$ is the change in work function caused by an increase in the concentration of low electronegativity cations, and $\Delta\phi_d$ is the change in work function cause by increase in density of donor states. The term $\Delta\phi_\chi$ accounts for the gradual linear decline in work function and the term $\Delta\phi_d$ accounts for the initial rapid decrease in work function with O-deficiency.

In order to derive expressions that relate $\Delta\phi_\chi$ and $\Delta\phi_d$ to the degree of non-stoichiometry, we start by writing the O-vacancy formation reaction using Kröger-Vink notation:

$$O_O^x + 2M_M^x \rightarrow v_O^{\bullet\bullet} + 2M_M^{/} + \frac{1}{2}O_{2(g)} \tag{4}$$

where $O_O{}^x$ represents an oxygen ion on its regular lattice site, $M^x{}_M$ represents a metal ion on its regular lattice site and with the charge it would have in the stoichiometric lattice, v_Oö represents a doubly positive charged oxygen vacancy, and $M^{/}{}_M$ represents a metal cation on its regular lattice site, but with an extra electron relative to what it would have in the stoichiometric

oxide. In the case of MoO_3, we can rewrite this reaction as follows:

$$O_O^x + 2Mo^{6+} \rightarrow v_O^{\bullet\bullet} + 2Mo^{5+} + \frac{1}{2}O_{2(g)} \quad (5)$$

For MoO_{3-x}, where x represents the degree of oxygen deficiency, we have the equality $[Mo^{5+}] = 2x$. From this expression, we see that each O-vacancy gives rise to two Mo^{5+} cations, and the disappearance of two Mo^{6+} cations

2.5.1. Electronegativity

As Mo^{5+} has a lower electronegativity than Mo^{6+}, the work function of O-deficient MoO_3 will decrease with increasing Mo^{5+} concentration. Using Nethercott's postulate of geometric mean[32] to write the group electronegativity of MoO_{3-x}, we can write an expression for the Fermi level dependence on non-stoichiometry (x). This yields the following equation for the Fermi level of MoO_{3-x}:

$$E_F = \left((\chi_{Mo^{6+}})^{1-2x}(\chi_{Mo^{5+}})^{2x}(\chi_{O^{2-}})^{3-x}\right)^{1/(4-x)} \quad (6)$$

where $\chi_{Mo^{6+}}$, $\chi_{Mo^{5+}}$ and $\chi_{O^{2-}}$ are the electronegativities of Mo^{6+}, Mo^{5+} and O^{2-}, respectively. This equation gives a linear relation between E_F and O-vacancy concentration, as shown in Figure 6b.

2.5.2. Donor States

While the linear contribution of Figure 6a can be accounted for using electronegativity arguments, the work function versus O-deficiency trend also exhibits an initial rapid decrease in work function. This rapid initial work-function decrease was also seen for TiO_2 and WO_3 (see Supporting Information). We propose that the initial decrease is caused by an increase in donor-state concentration with increasing O-vacancy concentration.

In the UPS valence-band spectra, one can see that O-vacancies in MoO_3 give rise to donor states near the Fermi level. Donor states close to the conduction band will ionize, increasing the density of carriers in the conduction band, and give rise to an upward Fermi-level shift,[38] as illustrated in **Figure 7**. Donor states from O-vacancy defects are also present in the near-stoichiometric oxide; however, they are present at a concentration that is below the detection limit of UPS (we estimate, using a O-vacancy formation energy of ≈0.55 eV,[52,53] that x in near-stoichiometric MoO_{3-x} is $\approx 5 \times 10^{-7}$).

The small number of defects in near-stoichiometric MoO_3 is sufficient to push the Fermi level close to the conduction band. However, based on experimental values of valence and conduction band positions,[15,21,23] as well as calculations of Fermi level position (shown below), the Fermi level of near-stoichiometric MoO_3 should not yet be pinned to the conduction band.

The reported electronic bandgap of MoO_3 is between 3.0 and 3.2 eV (based on UPS and IPES).[15,21,23] Therefore, from our UPS spectrum of near-stoichiometric MoO_3, where the valence band maximum (VBM) is 9.5 eV below the vacuum level, the conduction band would be between 6.5 eV and 6.3 eV below the vacuum level. With a work function of 6.89 eV, the Fermi level

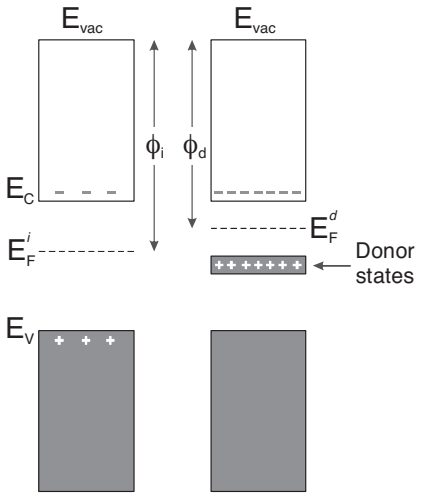

Figure 7. Schematic energy-level diagrams of a stoichiometric d^0 oxide (left) and an O-deficient d^0 oxide (right), illustrating how ionized donor states shift the Fermi level (E_F) closer to the conduction vacuum level (E_{vac}), resulting in a decrease in work function (φ). E_F^i, and E_F^d are the Fermi levels of the stoichiometric and defective oxides. E_c and E_v are the conduction band minimum and valence band maximum energies, respectively.

of near-stoichiometric MoO_3 would be ≈0.39–0.59 eV below the conduction band minimum (CBM). An accurate representation of MoO_3's band positions based on UPS and IPES is provided in the Supporting Information.

In the following discussion, we argue that near-stoichiometric MoO_3, having a very high work function (≈6.89 eV), has a defect density such that a slight increase in defect density results in a steep decrease in work function. We start by writing an equation that relates the electron density in the conduction band to the position of the Fermi level (relative to the conduction band):[35]

$$E_F - E_c = -kT\ln\left(\frac{n^e}{N_c}\right) \quad (7)$$

where E_F is the Fermi energy, E_c is the energy of the conduction band minimum, n^e is the concentration of electrons in the conduction band, N_c is the effective density of states of the conduction band minimum, k is the Boltzmann constant and T is the absolute temperature.

The concentration of free carriers in the conduction band would be the sum of contributions from the VBM (the O 2p band) and the defect band. The free carrier concentrations can be calculated using the following equation.[38]

$$n^e = \sqrt{N_v N_c \exp\left[\frac{-E_g}{kT}\right]} \quad (8)$$

where N_v is the effective density of states of the valence level, N_c is the effective density of states of the conduction band, E_g is the bandgap. By combining Equation (8) and (9) we arrive at the following equation for Fermi level position relative to the conduction band:

$$E_F - E_c = -\frac{1}{2}kT\ln\left(\frac{N_v}{N_c}\exp\left[\frac{-E_g^{(0)}}{kT}\right] + \frac{N_d}{N_c}\exp\left[\frac{-E_g^{(d)}}{kT}\right]\right) \quad (9)$$

where N_v is the effective density of states of the O 2p band, N_d is the effective density of states of the defect band, $E_g^{(0)}$ is the energy gap between the O 2p band and the conduction band (ca. 3–3.2 eV), and $E_g^{(d)}$ is the gap between the defect band and the conduction band (ca. 0.8 eV).

The density of donor states, N_d, will be proportional to the density of Mo^{5+} cations, so we will substitute $[Mo^{5+}]$ for N_d in Equation (9). A plot of work function versus non-stoichiometry (x in MoO_{3-x}) from Equation (9) is shown in Figure 6c. We have used $E_c = 6.3$ eV, $E_g^{(0)} = 3.2$ eV and $E_g^{(d)} = 0.8$ eV.

In order to estimate where near-stoichiometric MoO_3 should be on this curve, we need estimate the Mo^{5+} concentration in near-stoichiometric MoO_3. Using the defect reaction shown in Equation (5), we can write the following equilibrium constant:

$$K = \frac{\left[v_O^{\bullet\bullet}\right]\left[Mo^{5+}\right]^2}{\left[O_O^x\right]\left[Mo^{6+}\right]^2}p_{O_2}^{1/2} \quad (10)$$

In the case of dilute defects, the denominator of the above equation will be approximately unity. Furthermore, we can use the relation $[Mo^{5+}] = 2[v_O\ddot{o}]$ to obtain the following equation for Mo^{5+} concentration:

$$\left[Mo^{5+}\right] = 2^{1/2}\exp\left[\frac{-\Delta H_{v_O}}{3kT}\right]p_{O_2}^{-1/6} \quad (11)$$

where ΔH_{vO} is the enthalpy of formation for oxygen vacancies, and p_{O_2} is the oxygen partial pressure. One can estimate ΔH_{vO}, using the approximation proposed by Kofstad, which uses sublimation and formation enthalpies.[52] From this approximation, we get a value for ΔH_{vO} of ≈0.55 eV, and an Mo^{5+} atomic concentration of 1×10^{-4} (or $x \approx 5 \times 10^{-7}$). For this calculation we used $T = 850$ K (the MoO_3 deposition temperature). Note that we have used $p_{O_2} = 1$ in this estimate, as the equilibrium with background oxygen in the vacuum chamber is expected to be slow relative to our preparation and measurement time.

According to these calculations, the increase in donor-state density can account for an initial rapid drop in work function of ca. 0.15 eV. This is consistent with the experimental valence band and conduction band positions, within experimental error. The near-stoichiometric oxide is on the steep region of the logarithmic relationship shown in Figure 6c. Thus, for near-stoichiometric oxides, the work function decreases very rapidly. Once the defect states are within the detection limit of UPS (i.e., at $x \approx 0.01$) the work function is already on the shallow-slope region of the logarithmic curve in Figure 6c and Fermi level becomes insensitive to donor-state concentration.

In order to obtain a complete equation relating MoO_3 work function to non-stoichiometry we can make one further approximation. The conduction band is much further from the O 2p band than it is from the defect band. Thus the carriers contributed from the O 2p band will be several orders of magnitude less than those contributed from the defect band. Thus we can neglect the carriers from the O 2p band to arrive at an equation relating $\Delta\varphi$ with $[Mo^{5+}]$:

$$\Delta\phi_d = -\frac{1}{2}kT\ln\left(\frac{\left[Mo^{5+}\right]^{(d)}}{\left[Mo^{5+}\right]^{(0)}}\right) \quad (12)$$

where $[Mo^{5+}]^{(d)}$ is the concentration of Mo^{5+} in the defective oxide and $[Mo^{5+}]^{(0)}$ is the Mo^{5+} concentration in the near-stoichiometric oxide. Note that the terms N_c and E_g from Equation (8) have cancelled each other out to get Equation (10). We have also made the assumption that the donor-state energy, valence band energy, and conduction band energy remain constant as $[Mo^{5+}]$ increases. This assumption does not hold at high O-vacancy concentrations.

We can now write a complete equation that relates work function to oxygen deficiency by using Equation (6), (11), and (3), and by changing $[Mo^{5+}]$ to O-deficiency (x).

$$\phi = \phi_0 + \left[\left(\left(\chi_{Mo^{6+}}\right)^{1-2x}\left(\chi_{Mo^{5+}}\right)^{2x}\left(\chi_{O^{2-}}\right)^{3-x}\right)^{1/(4-x)}\right] + \left[-\frac{1}{2}kT\ln\left(\frac{x}{x_0}\right)\right] \quad (13)$$

where ϕ is the work function of the O-deficient oxide, ϕ_0 is the work function of the reference near-stoichiometric oxide, x is the O-deficiency of the defective oxide, x_0 is the O-deficiency of the reference oxide and $\Delta x = x - x_0$. Equation (14) is shown in Figure 6a as the dashed blue line. We used ionic electronegativity values from Campet et al.[39] and converted to units of eV. Electronegativity values of 6.4 eV for Mo^{6+}, 5.4 eV for Mo^{5+}, and 11.3 eV for O^{2-} were used. The non-stoichiometry of the near-stoichiometric oxide was calculated to be $x_0 = 5 \times 10^{-7}$, using an O-vacancy formation energy of 0.55 eV and a T_0 of 850 K (the MoO_3 deposition temperature).

The range for which the dilute-defects model applies depends on the details of the oxide. Defects interact with one another, and cluster together and form line defects or shear planes that can eliminate some of the oxygen vacancies.[54] For example, MoO_3 forms Magnéli phases via shear planes.[55] Consequently, it is not trivial to determine the O-vacancy and Mo^{5+} concentration from the Mo:O ratio.

Furthermore, as oxygen is continually removed additional oxidation states form and new phases become stable. The stability ranges for oxides differ from one to another. The equations presented that relate O-vacancy concentration and work function apply when reduction gives rise to only one new oxidation state (i.e., $Mo^{6+} \rightarrow Mo^{5+}$). To construct an equation that relates non-stoichiometry to work function when additional oxidation states begin to form, one must incorporate a relationship between oxygen vacancy concentration and the concentrations of other oxidation states.

2.6. Non-Dilute Oxygen Vacancies

At very high O-vacancy concentrations, an oxide can become completely reduced to a new stable phase. The oxide's crystal structure and electronic structure completely change from what

they were in the fully oxidized form. The relationship between electron chemical potential and O-deficiency at high O-vacancy concentrations becomes more complex.

In the cases of dilute O-vacancies, the donor state energy stays constant as the O-vacancy concentration increases; however, in the cases of high O-vacancy concentrations, changes to the oxide's crystal structure result in different metal-oxygen bond lengths and coordination symmetries. These structural changes result in changes to the valence band positions. Furthermore, the metal cations become reduced and thus become occupied with additional electrons. The additional electrons fill additional valence states, and result in new occupied valence features.

Figure 8 shows photoemission spectra of MoO_3 as it is reduced to MoO_2. MoO_3 has orthorhombic crystal symmetry and is a wide-bandgap semiconductor, while MoO_2 has monoclinic crystal symmetry and is a metallic oxide.

Fully oxidized MoO_3 contains only Mo^{6+} cations. O-vacancy defects cause Mo^{5+} to appear, and after a certain vacancy concentration, Mo^{4+} cations begin to form, as seen in Figure 8a. One can consider the Mo^{5+} cations to have singly occupied d-bands, and Mo^{4+} cations to have doubly occupied d-bands. The valence spectra in Figure 8c show that the appearance of Mo^{5+} coincides with the appearance of the valence state labeled d_1. The appearance of Mo^{4+} coincides with an additional valence state labeled d_2. As the O-vacancy concentration increases, these valence features broaden and shift to lower binding energy. These changes are likely the result of the different crystal structure and Mo-O bond lengths of the MoO_2-like structure. Eventually the d_1 feature crosses the Fermi level, and thus the oxide becomes metallic.

The changes to an oxide's valence structure at high O-vacancy concentrations complicate the considerations for calculating the effects of donor states on work function. An accurate relationship between O-deficiency and work function at high O-vacancy concentrations is not expected to be simple, as one must incorporate a relationship between M-O bond length, coordination geometry and O-deficiency in order to account for the changes in donor state densities and binding energies. However, the relationship between work function and electronegativity remains straight-forward, and is expected to follow a linear trend. The lower electronegativity of the reduced cations still has the dominating effect of decreasing the oxide's work function, as seen in Figure 8d.

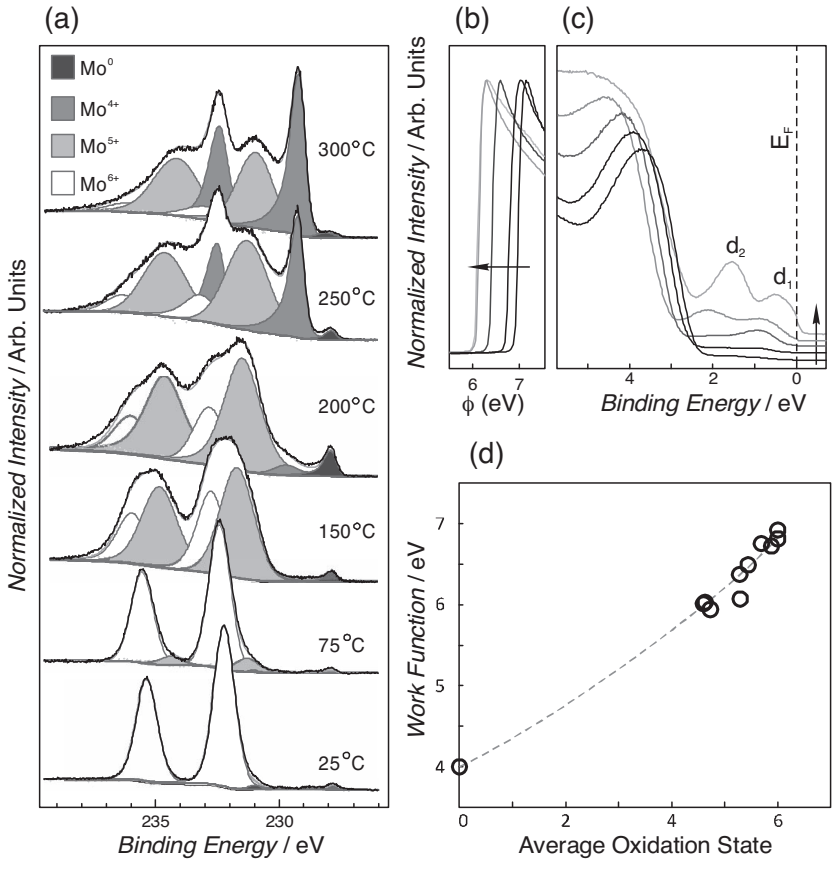

Figure 8. Photoemission spectra of an MoO_3 film as it is thermally reduced to MoO_2: a) Mo 3d XPS spectra, with components from Mo^{6+}, Mo^{5+}, Mo^{4+}, and Mo^0 indicated; b) secondary-electron cut-off; c) UPS valence spectra; and d) plot of work function versus average Mo oxidation state for MoO_3. The labels d_1 and d_2 in (d) indicate gap states from filling of Mo 4d states. The arrows in (c,d) indicate the direction of increasing temperature. The Fermi level is labeled E_F in (d). The dashed line in (d) is a guide to the eye.

2.7. Work Function and Defects Near an Interface

In many applications that use oxides, oxides take the form of thin films or nanoparticles that are in contact with a metal. We have observed that, for oxide thin films grown on metal substrates, an oxide's work function depends on its thickness. In general, oxide work function increases with distance from a metal/metal-oxide interface. Here we demonstrate this behavior using MoO_3 films grown by oxidation of Mo. Photoemission spectra of these films are shown in **Figure 9**. The XPS spectra show that, as the film thickens, the Mo^{6+} signal increases, the Mo^0 peak diminishes and there is evidence of Mo^{5+} species within the first few nanometers of the Mo/MoO_3 interface.

The UPS spectra show further evidence of reduced Mo. The valence spectra in Figure 9b,c show that donor states are present at the Mo/MoO_3 interface (labelled d_1 and d_2). The d_2 feature, which is associated with doubly occupied Mo 4d states, is only present within the first ≈1 nm of the interface. The d_1 feature, which is associated with singly occupied Mo 4d states persists for several nanometers from the interface, and eventually diminishes. The decrease in defect-state intensity is concurrent with an increase in work function.

Figure 9d shows a plot of work function versus oxide thickness. This plot shows that the work function can vary by ≈1 eV simply by changing the oxide's thickness. This

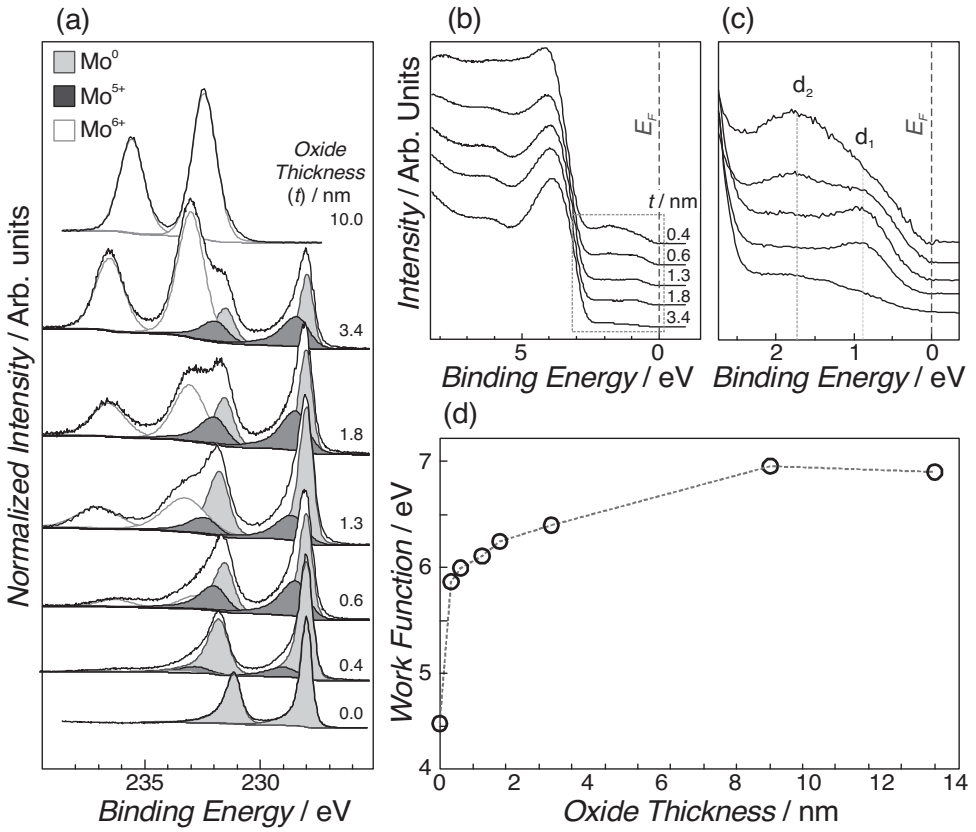

Figure 9. Photoemission spectra of various MoO_3 film thicknesses for a MoO_3 film grown by oxidation of Mo: a) Mo 3d spectra, b) UV photoemission valence spectra, and c) expanded view of the shallow valence features. The labels d_1 and d_2 indicate defect states. d) Plot of work function versus MoO_3 film thickness.

observation can explain some of the variation in reported work function values in the literature. The work function of MoO_3 eventually reaches a plateau of ≈6.9 eV. This value is expected to be the upper limit for MoO_3, as O-vacancy defects and atmospheric adsorbates will decrease the work function.

We have observed similar behavior, that work function increases with oxide thickness, for all the oxides examined in this work. The work function values shown in Figure 2 are measured from oxide films that are thick enough such that the underlying metal signal cannot be detected with XPS (implying film thicknesses of >10 nm in most cases).

For most transition metals that have multiple stable oxides, the high-oxidation-state form is not thermodynamically stable in contact with the parent metal. In such scenarios, low oxidation-state oxides are expected to be present at the metal/metal-oxide interface. For example, in the Mo-O phase diagram, one will find that there is no region where MoO_3 and Mo are in equilibrium together. Instead, MoO_2 and Mo equilibrate, and as a result, MoO_3 thin films grown on Mo have an interfacial layer that is MoO_2-like. This type of behaviour is expected for many other metal/metal-oxide systems, such as $Cu/Cu_2O/CuO$, $Ti/TiO/TiO_2$, $V/VO/V_2O_3/V_2O_5$. Indeed there have been previous reports of reduced metal cations at metal/metal-oxide interfaces. We expect that these reduced cations also result in work function lowering, and influence the oxide thicknesses needed for certain applications.

In applications such as organic electronics, where oxide layers need to be thin in order to minimize series resistance, the decreased work function of an oxide near a metal/oxide interface may forfeit the oxide's favourable energy-level alignment with organic semiconductors. In this case, it may be necessary to make a thicker oxide film or change to a different oxide altogether.

3. Conclusion

We have shown that transition metal oxide work functions are correlated to average cation oxidation state. As cation oxidation state is also related to point defect concentrations—such as oxygen vacancy concentrations—transition metal oxide work functions can be altered by small deviations from stoichiometry. We have found that work functions tend to decrease with decreasing cation oxidation state. Consequently, removal of oxygen results in a decrease in work function. We attributed this behavior to two main contributions: 1) the lower electronegativity of lower-oxidation-state cations and 2) the increase in valence donor states with decreasing cation oxidation state. Using these concepts, we have presented a model that describes the relationship between work function and oxygen vacancy concentration for d^0 oxides in the dilute limit. In the case of high O-vacancy concentrations, where the oxide approaches complete reduction, we have discussed why changes to the oxide's crystal

structure cause the valence state contribution to work function to complex, yet the cation electronegativity contribution still has a dominant effect on an oxide's work function.

These findings have implications to oxide thin films used in devices and oxide nanoparticles in contact with metals.

4. Experimental Section

Photoemission spectra were collected using a Physical Electronics 5500 Multi-Technique system, using monochromated Al Kα radiation ($h\nu$ = 1486.7 eV) for XPS spectra and non-monochromated He Iα radiation ($h\nu$ = 21.22 eV) for UPS spectra and work function measurements. XPS spectra were collected using a take-off angle of 75°. UPS spectra and work function measurements were measured at a take-off angle of 88°. During UPS and work function measurements, the sample was held at a negative bias of –15 V relative to the spectrometer.

The MoO_3 films used for the dilute defects experiments were grown by vacuum sublimation of 99.99% pure MoO_3 powder from a 10 cc cone-shaped alumina crucible and placed in a Knudsen cell. MoO_3 was evaporated at a temperature of 550 °C to obtain a deposition rate of ≈0.3 Å/s at the sample surface, as monitored by an oscillating quartz thickness monitor. Substrates were ≈1 cm × 1 cm Si wafers coated with 200 nm of Mo metal. The MoO_3 evaporation source was positioned 31 cm away from the sample, at an angle of 35° (K-cell axis relative to sample normal). The pressure during deposition was $\approx 5 \times 10^{-9}$ torr.

The oxide films used for the work function measurements (shown in Figure 2) were prepared by metal oxidation. Metal films were initially coated onto polished, degenerately-doped p-type Si wafers by magnetron sputter deposition from 99.99% pure metal targets. The metal films were ≈200 nm thick. All metal films were sputter cleaned in the XPS chamber to remove atmospheric contamination and the native oxide films prior to oxidation. The sputter-cleaned metal films were then moved (without exposure to air) to an attached oxidation chamber, having a base pressure of $\approx 5 \times 10^{-9}$ torr. The oxidation chamber was back-filled with ≈760 torr of high-purity O_2 and oxidized for 3–5 hours. During oxidation, samples were heated up to ~ 300 °C using a 600 W halogen light bulb, positioned ≈2 cm away from the sample surface. Ultraviolet light was shone through a quartz window during oxidation to increase the oxidizing power of the gas by generating O_3. This allowed more rapid oxide growth and high-oxidation-state oxides to be obtained. This procedure provided carbon-free and hydroxide-free oxide thin films between 5 nm and 15 nm thick (depending on the metal's oxidation rate).

Reduced oxides were prepared by vacuum annealing the oxidized metals. The pressure during annealing ranged from $\approx 5 \times 10^{-9}$ to 1×10^{-8} torr. The samples were heated using a 600 W halogen light bulb. Temperatures ranged from 100 °C to 400 °C depending on the oxide. Oxides were annealed for 6–12 h.

Oxygen vacancy defects were induced by Xe^+ ion bombardment using a Physical Electronics 04-303 Ion Gun, using a Physical Electronics 11-065 controller. The ion beam was set to a 1 mm diameter spot size and raster area of 8 mm × 8 mm. For MoO_3 and TiO_2, a beam voltage of 0.5 kV was used. The ion current at the sample was ≈0.5 μA. Samples were sputtered in 5 s intervals. Due to the faster sputter rate of O^{2-}, differential sputtering occurs and results in a gradual increase in O-vacancy concentration.

Supporting Information

Supporting Information is available from the Wiley Online Library or from the author.

Acknowledgements

The research of Z.H. is funded from the National Science and Research Council (NSERC) of Canada. M.T.G. and M.G.H. are grateful for scholarships from NSERC. All authors gratefully acknowledge NSERC's support.

Received: March 4, 2012
Revised: May 23, 2012
Published online: June 26, 2012

[1] a) K. Tanabe, W. F. Holderich, *Appl. Catal. A-Gen.* **1999**, *181*, 399; b) H. H. Kung, *Transition Metal Oxides: Surface Chemistry and Catalysis*, Vol. *45*, Elsevier, New York **1989**.
[2] S. C. Roy, O. K. Varghese, M. Paulose, C. A. Grimes, *ACS Nano* **2010**, *4*, 1259.
[3] a) C. F. Qiu, Z. L. Xie, H. Y. Chen, M. Wong, H. S. Kwok, *J. Appl. Phys.* **2003**, *93*, 3253; b) D. Kabra, L. P. Lu, M. H. Song, H. J. Snaith, R. H. Friend, *Adv. Mater.* **2010**, *22*, 3194; c) J. Meyer, R. Khalandovsky, P. Gorrn, A. Kahn, *Adv. Mater.* **2011**, *23*, 70; d) E. A. Gibson, A. L. Smeigh, L. Le Pleux, J. Fortage, G. Boschloo, E. Blart, Y. Pellegrin, F. Odobel, A. Hagfeldt, L. Hammarstrom, *Angew. Chem. Int. Ed.* **2009**, *48*, 4402; e) A. Nattestad, A. J. Mozer, M. K. R. Fischer, Y. B. Cheng, A. Mishra, P. Bauerle, U. Bach, *Nat. Mater.* **2010**, *9*, 31; f) B. O'Regan, M. Grätzel, *Nature* **1991**, *353*, 737.
[4] a) A. Jablonski, K. Wandelt, *Surf. Interf. Anal.* **1991**, *17*, 611; b) N. Koch, *ChemPhysChem* **2007**, *8*, 1438; c) S. Braun, W. R. Salaneck, M. Fahlman, *Adv. Mater.* **2009**, *21*, 1450.
[5] I. T. Steinberger, K. Wandelt, *Phys. Rev. Lett.* **1987**, *58*, 2494.
[6] J. Meyer, K. Zilberberg, T. Riedl, A. Kahn, *J. Appl. Phys.* **2011**, 110.
[7] M. T. Greiner, M. G. Helander, W. M. Tang, Z. B. Wang, J. Qiu, Z. H. Lu, *Nat. Mater.* **2012**, *11*, 76.
[8] S. Lany, J. Osorio-Guillen, A. Zunger, *Phys. Rev. B* **2007**, *75*, 241203.
[9] V. E. Henrich, P. A. Cox, *The Surface Science of Metal Oxides*, Cambridge University Press, Cambridge **1994**.
[10] a) K. Wandelt, *Appl. Surf. Sci.* **1997**, *111*, 1; b) H. Ishii, K. Sugiyama, E. Ito, K. Seki, *Adv. Mater.* **1999**, *11*, 605.
[11] a) D. E. Eastman, *Phys. Rev. B* **1970**, *2*, 1; b) H. B. Michaelson, *J. Appl. Phys.* **1950**, *21*, 536.
[12] V. E. Henrich, P. A. Cox, *The Surface Science of Transition Metal Oxides*, Cambridge University Press, Cambridge **1994**, Ch. 1, pp. 7–13.
[13] R. Smoluchowski, *Phys. Rev.* **1941**, *60*, 661.
[14] W. Li, D. Y. Li, *J. Chem. Phys.* **2005**, *122*, 064708.
[15] Irfan H. Ding, Y. Gao, C. Small, D. Y. Kim, J. Subbiah, F. So, *Appl. Phys. Lett.* **2010**, *96*, 243307.
[16] M. T. Greiner, M. G. Helander, Z.-B. Wang, W.-M. Tang, Z.-H. Lu, *J. Phys. Chem. C* **2010**, *114*, 19777.
[17] D. O. Scanlon, G. W. Watson, D. J. Payne, G. R. Atkinson, R. G. Egdell, D. S. L. Law, *J. Phys. Chem. C* **2010**, *114*, 4636.
[18] M. Krjöger, S. Hamwi, J. Meyer, T. Riedl, W. Kowalsky, A. Kahn, *Appl. Phys. Lett.* **2009**, *95*, 123301.
[19] J. Meyer, M. Kröger, S. Hamwi, F. Gnam, T. Riedl, W. Kowalsky, A. Kahn, *Appl. Phys. Lett.* **2010**, *96*, 193302.
[20] a) Q. Y. Bao, J. P. Yang, Y. Q. Li, J. X. Tang, *Appl. Phys. Lett.* **2010**, *97*, 063303; b) Q. Y. Bao, J. P. Yang, J. X. Tang, Y. Q. Li, C. S. Lee, S. T. Lee, *Org. Electron.* **2010**, *11*, 1578; c) S. Hamwi, J. Meyer, T. Winkler, T. Riedl, W. Kowalsky, *Appl. Phys. Lett.* **2009**, *94*, 253307; d) J. Meyer, T. Winkler, S. Hamwi, S. Schmale, H. H. Johannes, T. Weimann, P. Hinze, W. Kowlasky, T. Riedl, *Adv. Mater.* **2008**, *20*, 3839; e) Y. H. Kim, S. Kwon, J. H. Lee, S. M. Park, Y. M. Lee, J. W. Kim, *J. Phys. Chem. C* **2011**, *115*, 6599; f) S. Y. Chiam, B. Dasgupta, D. Soler, M. Y. Leung, H. Liu, Z. E. Ooi, L. M. Wong, C. Y. Jiang, K. L. Chang, J. Zhang, *Sol. Energy Mater. Sol. Cells* **2012**, *99*, 197; g) H. Lee, S. W. Cho, K. Han, P. E. Jeon, C. N. Whang, K. Jeong, K. Cho, Y. Yi, *Appl. Phys. Lett.* **2008**, *93*, 043308; h) Y. Yi,

P. E. Jeon, H. Lee, K. Han, H. S. Kim, K. Jeong, S. W. Cho, *J. Chem. Phys.* **2009**, *130*, 094704.
[21] K. Kanai, K. Koizumi, S. Ouchi, Y. Tsukamoto, K. Sakanoue, Y. Ouchi, K. Seki, *Org. Electron.* **2010**, *11*, 188.
[22] M. V. Ganduglia-Pirovano, A. Hofmann, J. Sauer, *Surf. Sci. Rep.* **2007**, *62*, 219.
[23] M. Kröger, S. Hamwi, J. Meyer, T. Riedl, W. Kowalsky, A. Kahn, *Org. Electron.* **2009**, *10*, 932.
[24] T. Matsushima, G. H. Jin, Y. Kanai, T. Yokota, S. Kitada, T. Kishi, H. Murata, *Org. Electron.* **2011**, *12*, 520.
[25] a) M. T. Greiner, M. G. Helander, Z. B. Wang, W. M. Tang, J. Qiu, Z. H. Lu, *Appl. Phys. Lett.* **2010**, *96*, 213302; b) M. Vasilopoulou, L. C. Palilis, D. G. Georgiadou, A. M. Douvas, P. Argitis, S. Kennou, L. Sygellou, G. Papadimitropoulos, I. Kostis, N. A. Stathopoulos, D. Davazoglou, *Adv. Funct. Mater.* **2011**, *21*, 1489; c) M. Vasilopoulou, G. Papadimitropoulos, L. C. Palilis, D. G. Georgiadou, P. Argitis, S. Kennou, I. Kostis, N. Vourdas, N. A. Stathopoulos, D. Davazoglou, *Org. Elect.* **2012**, *13*, 796; d) M. Vasilopoulou, L. C. Palilis, D. G. Georgiadou, S. Kennou, I. Kostis, D. Davazoglou, P. Argitis, *Appl. Phys. Lett.* **2012**, *100*, 013311.
[26] R. T. Sanderson, *Science* **1951**, *114*, 670.
[27] I. D. Brown, A. Skowron, *J. Am. Chem. Soc.* **1990**, *112*, 3401.
[28] J. C. Phillips, *Phys. Rev. Lett.* **1968**, *20*, 550.
[29] K. Y. Li, D. F. Xue, *Mater. Res. Bull.* **2010**, *45*, 288.
[30] a) K. Y. Li, Z. S. Ding, D. F. Xue, *Phys. Status Solidi B* **2011**, *248*, 1227; b) K. Y. Li, X. T. Wang, F. F. Zhang, D. F. Xue, *Phys. Rev. Lett.* **2008**, *100*, 235504; c) K. Y. Li, P. Yang, D. F. Xue, *Acta Mater.* **2012**, *60*, 35.
[31] W. Gordy, W. J. O. Thomas, *J. Chem. Phys.* **1956**, *24*, 439.
[32] A. Nethercott, *Phys. Rev. Lett.* **1974**, *33*, 1088.
[33] a) E. C. M. Chen, W. E. Wentworth, J. A. Ayala, *J. Chem. Phys.* **1977**, *67*, 2642; b) K. W. Frese, *J. Vac. Sci. Technol.* **1979**, *16*, 1042; c) R. T. Poole, D. R. Williams, J. D. Riley, J. G. Jenkin, J. Liesegang, R. C. G. Leckey, *Chem. Phys. Lett.* **1975**, *36*, 401.
[34] K. Y. Li, D. F. Xue, *J. Phys. Chem. A* **2006**, *110*, 11332.
[35] S. Yamamoto, *Rep. Prog. Phys.* **2006**, *69*, 181.
[36] a) R. S. Mulliken, *J. Chem. Phys.* **1934**, *2*, 782; b) R. S. Mulliken, *J. Chem. Phys.* **1935**, *3*, 573.
[37] R. G. Parr, R. A. Donnelly, M. Levy, W. E. Palke, *J. Chem. Phys.* **1978**, *68*, 3801.
[38] D. Neamen, in *Semiconductor Physics and Deveices*, McGraw-Hill, New York **2003**.
[39] G. Campet, J. Portier, M. A. Subramanian, *Mater. Lett.* **2004**, *58*, 437.
[40] S. F. Matar, G. Campet, M. A. Subramanian, *Prog. Solid State Chem.* **2011**, *39*, 70.
[41] K. Y. Li, D. F. Xue, *Chin. Sci. Bull.* **2009**, *54*, 328.
[42] Y. G. Zhang, *Inorg. Chem.* **1982**, *21*, 3886.
[43] J. A. Duffy, *J. Sol. St. Chem.* **1986**, *62*, 145.
[44] T. Uozumi, K. Okada, A. Kotani, *J. Phys. Soc. Jpn.* **1993**, *62*, 2595.
[45] S. Laubach, P. C. Schmidt, A. Thissen, F. J. Fernandez-Madrigal, Q. H. Wu, W. Jaegermann, M. Klemm, S. Horn, *Phys. Chem. Chem. Phys.* **2007**, *9*, 2564.
[46] R. Zimmermann, P. Steiner, R. Claessen, F. Reinert, S. Hüfner, P. Blaha, P. Dufek, *J. Phys.-Condens. Matter* **1999**, *11*, 1657.
[47] H. J. Zhai, S. Li, D. A. Dixon, L. S. Wang, *J. Am. Chem. Soc.* **2008**, *130*, 5167.
[48] J. Vanelp, J. L. Wieland, H. Eskes, P. Kuiper, G. A. Sawatzky, F. M. F. Degroot, T. S. Turner, *Phys. Rev. B* **1991**, *44*, 6090.
[49] L. Soriano, M. Abbate, D. Alders, J. M. Sanz, *Solid State Commun.* **1994**, *91*, 551.
[50] a) M. Shimoda, T. Hirata, K. Yagisawa, M. Okochi, A. Yoshikawa, *J. Mater. Sci. Lett* **1989**, *8*, 1089; b) W. Grunert, A. Y. Stakheev, R. Feldhaus, K. Anders, E. S. Shpiro, K. M. Minachev, *J. Phys. Chem.* **1991**, *95*, 1323; c) M. Yamada, J. Yasumaru, M. Houalla, D. M. Hercules, *J. Phys. Chem.* **1991**, *95*, 7037.
[51] R. Tokarz-Sobieraj, K. Hermann, M. Witko, A. Blume, G. Mestl, R. Schlögl, *Surf. Sci.* **2001**, *489*, 107.
[52] P. Kofstad, *J. Phys. Chem. Sol.* **1967**, *28*, 1842.
[53] W. Thoni, P. B. Hirsch, *Philos. Mag.* **1976**, *33*, 639.
[54] a) J. S. Anderson, B. G. Hyde, *J. Phys. Chem. Sol.* **1967**, *28*, 1393; b) P. L. Gai, *Philos. Mag. A* **1981**, *43*, 841.
[55] A. Magnéli, *Acta Crystallogr.* **1953**, *6*, 495.